JPE 15-6-25

http://dx.doi.org/10.6113/JPE.2015.15.6.1654
ISSN(Print): 1598-2092 / ISSN(Online): 2093-4718

LCL Resonant Compensation of Movable ICPT Systems with a Multi-load

Jie Hua*, Hui-Zhen Wang†, Yao Zhao*, and Ai-Long Zou**

*,†Department of Automation Engineering, Nanjing University of Aeronautics and Astronautics, Nanjing, China
**724 Research Institute of China Shipbuilding Industry Corporation, Nanjing, China

Abstract

Compared to LC resonance, LCL resonance has distinct advantages such as a large resonant capability, low voltage and current stresses of the power device, constant voltage or current output characteristics, and fault-tolerance capability. Thus, LCL resonant compensation is employed for a movable Inductive Contactless Power Transfer (ICPT) system with a multi-load in this paper, which achieves constant current output characteristics. Peculiarly, the primary side adopts a much larger compensation inductor than the primary leakage inductor to lower the reactive power, reduce the input current ripple, generate a large current in the primary side, and realize soft-switching. Furthermore, this paper proposes an approximate resonant point for large inductor-ratio LCL resonant compensation through fundamental wave analysis. In addition, the PWM control strategy is used for this system to achieve constant current output characteristics. Finally, an experimental platform is built, whose secondary E-Type coils can ride and move on a primary rail. Simulations and experiments are conducted to verify the effectiveness and accuracy of both the theory and the design method.

Key words: Approximate resonant point, Constant-current characteristics, Large inductor-ratio, LCL resonant compensation, Movable ICPT system, Multi-load

NOMENCLATURE

f:	Input AC frequency
L:	Inductance value of resonant inductor L
L_a:	Inductance value of resonant inductor L_a
C:	Capacitance value of the resonant capacitor C
R:	Load resistance
λ:	$\equiv L_a/L$, ratio of inductors L_a and L
Q:	$\equiv \omega_o L/R$, the Q-value of the resonant circuit
Ω:	$\equiv 2\pi f$, the angular input frequency (in radians per second)
ω_o:	$\equiv 1/(LC)^{0.5}$, the angular resonant frequency (in radians per second)
ω_n:	$\equiv \omega/\omega_o$, the normalized angular frequency
Z_{in}:	Input impedance in the LCL resonance model
I_L:	RMS value of the output current in the LCL resonance model
U_o:	RMS value of the output voltage in the LCL resonance model
ω_{op}:	Approximate angular resonant frequency
L_{pc}:	Inductance value of the primary compensation inductor L_{pc}
L_p:	Inductance value of the primary leakage inductor L_p
C_p:	Capacitance value of the primary compensation capacitor C
ω_{op}:	$\equiv 1/(L_p C_p)^{0.5}$, the primary angular resonant frequency
ω_{np}:	$\equiv \omega/\omega_{op}$, the primary normalized angular frequency
λ_p:	$\equiv L_{pc}/L_p$, the ratio of inductors L_{pc} and L_p
Q_p:	$\equiv \omega_{op} L/R$, the Q-value of the resonant circuit
M_k:	Mutual inductance (k=1,2)
L_{sk}:	Inductance value of the secondary leakage inductor L_{sk} (k=1,2)

Manuscript received Jan. 28, 2015; accepted May 8, 2015
Recommended for publication by Associate Editor Jee-Hoon Jung.
†Corresponding Author: wanghz@nuaa.edu.cn
*Department of Automation Engineering, Nanjing University of Aeronautics and Astronautics, China
**The 724 Research Institute of China Shipbuilding Industry Corporation, China

Lsck: Inductance value of the secondary LCL compensation inductor Lsck (k=1,2)
Csk: Capacitance value of the secondary compensation capacitor Csk (k=1,2)
Rk: Secondary load resistance (k=1,2)
ωosk: ≡1/(LskCsk)0.5, the secondary angular resonant frequency (k=1,2)
ωnsk: ≡ω/ωosk, the secondary normalized angular frequency (k=1,2)
Qsk: ≡ωosk Lsk /Rk, the Q-value of the secondary side (k=1,2)
λsk: ≡Lsck/Lsk, the ratio of inductors Lsck and Lsk (k=1,2)
Zsk: Input impedance of the secondary side (k=1,2)
Zpsk: Equivalent secondary impedance in the primary side (k=1,2)
Req: Equivalent load in the primary side
Css: Capacitance value of the secondary series compensation capacitor Css
ωos: ≡1/(LskCss)0.5, the secondary angular resonant frequency of the series compensation
Uos: RMS value of the secondary output voltage with series compensation
Ip: RMS value of the primary rail current
Iosk: RMS value of the secondary output current (k=1,2)
Usk: RMS value of the secondary input voltage (k=1,2)
Pos: Output power of the secondary side with series compensation
PoLCLk: Output power of the secondary side with LCL compensation (k=1,2)
D: Duty cycle

I. INTRODUCTION

Based on the electromagnetic induction principle, Inductive Contactless Power Transfer (ICPT) systems transform power from the primary side of the coupling coils to the secondary side by converting electrical energy into magnetic energy. ICPT systems have a number of advantages such as high security performance and low maintenance cost. For example, eliminating the friction and spark caused by naked conductors, ICPT systems can enhance security and prolong the service life of trolley cars. It also has been the preferred power-delivery approach in many special applications, e.g., underwater and explosive environments. In addition, multi-load ICPT systems can supply power to a product line containing several electronic actuators with only one primary rail, which avoids the use of cables and improves the security performance. This paper focuses on constant-current-output movable ICPT systems with multi-loads, which are a good fit for magnet power supplies, capacitor charging power supplies, laser diode drivers, etc.

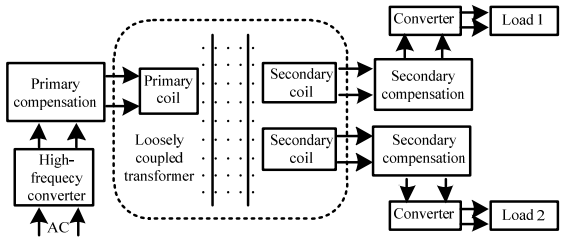

Fig. 1. The basic block diagram of movable ICPT system with multi-load.

The basic block diagram of a movable ICPT system with a multi-load is shown in Fig. 1. Through the rectifier and filter circuits, the power frequency source supply provides a constant dc voltage to the high-frequency inverter, which produces a high-frequency ac current in the primary coil and a high-frequency alternating magnetic field around the loosely coupled transformer. The secondary coils obtain energy from the magnetic field via an air gap and then induce alternating electromotive forces. At last, the alternating electromotive forces supply power for loads. It is important to note that one primary side coil can complete power transfer with multiple secondary coils at the same time.

To reduce the reactive power and losses caused by the low coupling coefficient of the coupling coils, it is essential to compensate movable ICPT systems. Parallel and series compensations are common and widely used in such systems [1]-[6]. However, series compensation is unsuitable for the primary side of a movable ICPT system due to its difficulty in generating a large primary current. Meanwhile, parallel compensation cannot meet the requirements of the secondary sides in multi-load or variable-load ICPT systems since its resonant frequency is related to the load resistor. To analyze and solve these problems, the fundamental wave analysis method is adopted for LC resonance [5], [6], which is also valuable for other resonance analyses. Furthermore, the stability, load range, and output power of ICPT systems are analyzed in [7].

Recently, many composite resonances have been put forward to overcome such defects as the low resonant capacity and high power device stress of LC resonance [8], [9]. However, among them only LCL resonant compensation with two similar-value inductors has been applied to movable ICPT systems [10]-[13]. Unlike the work in [14], this paper puts forward a large inductor-ratio LCL resonance to compensate the primary side of a movable ICPT system with a multi-load and a two-equal-inductor LCL resonance for the secondary side. Against analyzing a large-ratio LCL resonance comprehensively, an approximate resonant point is given out. The primary LCL compensation can lower reactive power, generate a large current in the primary side, suppress harmonic current and realize soft-switching. The secondary LCL compensation can increase output power and achieve a constant current output.

This paper is organized as follows. The analysis of LCL resonant compensation is first reviewed in Section II. Then, Section III presents the structure and model of a movable ICPT system with a multi-load as well as the design ideas and compensation requirements. Next, the design process of LCL resonant compensation is described in Section IV. Finally, the LCL compensation results and system characteristics are illustrated in Section V, and a summary is given in Section VI.

II. Analysis of the LCL Resonant Compensation

This section analyzes the effects of the normalized angular frequency ω_n and the ratio of the inductors λ on the LCL resonance characteristics. Then, an approximate resonant point is derived to simplify the system design, which can make the input impedance nearly pure resistive. In this case, the power factor can be significantly improved.

Fig. 2 shows a schematic diagram of an LCL circuit. Considering the fundamental wave only, the input impedance of the LCL circuit can be written as:

$$Z_{in} = \omega_o L \frac{1-\omega_n{}^2\lambda + j\omega_n Q\left[\lambda\left(1-\omega_n{}^2\right)+1\right]}{Q\left(1-\omega_n{}^2\right)+j\omega_n} \tag{1}$$

Furthermore, the inductance L current, i.e., output current, can be easily derived:

$$I_L = \frac{U_{in}}{\omega_o L}\frac{Q}{1-\omega_n{}^2\lambda + j\omega_n Q\left[\lambda\left(1-\omega_n{}^2\right)+1\right]} \tag{2}$$

Similarly, the resistance R voltage, i.e., output voltage, can be expressed as:

$$U_o = U_{in}\frac{1}{1-\omega_n{}^2\lambda + j\omega_n Q\left[\lambda\left(1-\omega_n{}^2\right)+1\right]} \tag{3}$$

A. Effects of ω_n

When ω_n is varying, the LCL circuit can present constant current (or voltage) output characteristics.

1) Constant Current Output Characteristic:

Considering $\omega_n = \sqrt{1/\lambda}$, (2) can be written as:

$$I_L\Big|_{\omega_n=\sqrt{\frac{1}{\lambda}}} = \frac{U_{in}}{j\omega_o L\sqrt{\lambda}} \tag{4}$$

It can be seen that the output current is unrelated to the load resistor, which means that is possesses the constant current output characteristic. Similarly, (1) can be derived as:

$$Z_{in}\Big|_{\omega_n=\sqrt{\frac{1}{\lambda}}} = \omega_o L\frac{jQ\sqrt{\lambda}}{Q\left(1-\frac{1}{\lambda}\right)+j\sqrt{\frac{1}{\lambda}}} \tag{5}$$

2) Constant Voltage Output Characteristic:

Substituting $\omega_n = \sqrt{1+1/\lambda}$ into (3) results in:

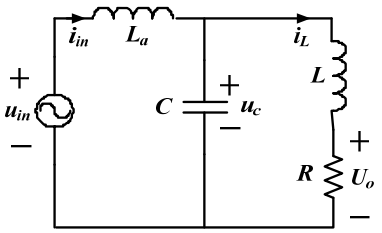

Fig. 2. LCL circuit diagram.

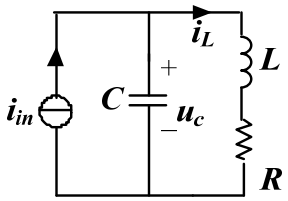

Fig. 3. The equivalent circuit of LCL with a large λ.

$$U_o\Big|_{\omega_n=\sqrt{1+\frac{1}{\lambda}}} = \frac{-U_{in}}{\lambda} \tag{6}$$

This shows that there is no relationship between the output voltage and the load resistor, i.e., the constant voltage output characteristic. Similarly, (1) can be derived as:

$$Z_{in}\Big|_{\omega_n=\sqrt{1+\frac{1}{\lambda}}} = \omega_o L\frac{\lambda^2}{Q-j\sqrt{\lambda(1+\lambda)}}. \tag{7}$$

B. Effects of λ

The ratio of the inductors λ influences the impedance characteristics and the equivalent circuit model of the LCL resonance circuit.

1) Input Impendence when λ=1:

Considering $\omega_n = \sqrt{1/\lambda}$, substituting λ=1 into (1) and (2) leads to the following equivalent expressions:

$$\begin{cases} I_L\Big|_{\lambda=1,\omega_n=1} = \dfrac{U_{in}}{j\omega_o L\sqrt{\lambda}} \\ Z_{in}\Big|_{\lambda=1,\omega_n=1} = \omega_o LQ \end{cases} \tag{8}$$

Obviously, when λ=1 and ω_n=1, the LCL circuit presents constant current output and pure resistive input impedance characteristics. However, the input impedance is inductive in the case of a constant voltage output, which can be seen from expression (7).

2) Equivalent Circuit Model when λ is large: With a large inductor L_a determined by λ (λ>10), the voltage source and inductor L_a, in Fig. 2, are equal to a current source, as shown in Fig. 3.

According to the equivalent circuit in Fig. 3, the approximate resonant angular frequency of the LCL resonant circuit is given below.

$$\omega_{op} = \frac{1}{\sqrt{LC}}\sqrt{1-\frac{CR^2}{L}} \tag{9}$$

where the resonant condition is:

$$R < \sqrt{L/C} \tag{10}$$

When operating at this approximate resonant angular frequency, the LCL circuit still can show great resonant characteristics, such as a pure resistive impedance characteristic.

III. Structure and Model of a Movable ICPT System with a Multi-load

A. Structure of a Movable ICPT System with a Multi-load

This section introduces the structure of a movable multi-load ICPT system and establishes the equivalent circuit model of a system with two loads.

As can be seen from Fig. 4, this movable ICPT system with a multi-load consists of a primary side and secondary sides (more than one). The primary side contains a rail, a primary compensation circuit, an inverter circuit and a DC voltage source. The secondary side is formed by a pick-up coil, a secondary compensation circuit and a load, which can move on a primary guide rail.

The secondary pick-up coil couples with the primary rail to form a loosely coupled transformer as the power transfer mechanism of the ICPT system, which can be regarded as a transformer with low coupling coefficient or two coupling inductors. An Ansoft 3-D model of the movable ICPT system is constructed in Fig. 5.

If one secondary E-Type coil moves along the rail in the Y direction, a mutual inductance between the primary side and the secondary side is almost constant since the magnetic field intensity is constant, which can be seen from Fig. 6(a). If the secondary side has an X-direction or Y-direction deviation, the mutual inductance will decrease and eventually both the primary and secondary resonance compensation will detune and the transfer power will drop. From Fig. 6(b), the central column of the E-Type coil has the strongest magnetic field. Therefore, it is assumed that the magnetic fields of the secondary sides will not influence each other and disturb the primary magnetic field.

B. Equivalent Circuit Model for a Movable ICPT System with a Multi-load

To simplify the modeling process, the fundamental wave analysis method is adopted to analyze and model this system. Firstly, the primary rail is considered as an inductor L_p. Secondly, the secondary pick-up coils are regarded as inductors L_{s1} and L_{s2} whose mutual inductances are M_1 and M_2. Finally, the dc source and inverter are replaced by an ac voltage source u_{in}. An equivalent circuit model of a movable ICPT system with two loads is given in Fig. 7(a).

The secondary input impedance can be written as:

$$Z_{s1} = \omega_{os1} L_{s1} \frac{1 - \omega_{ns1}\lambda_{s1} + j\omega_{ns1} Q_{s1}[\lambda_{s1}(1-\omega^2{}_{ns1}) + 1]}{Q_{s1}(1-\omega^2{}_{ns1}) + j\omega_{ns1}} \tag{11}$$

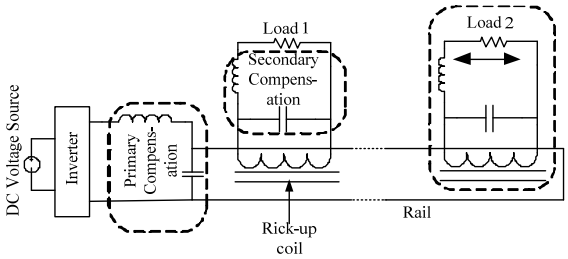

Fig. 4. The movable ICPT system with multi-load consisting of primary side and secondary sides.

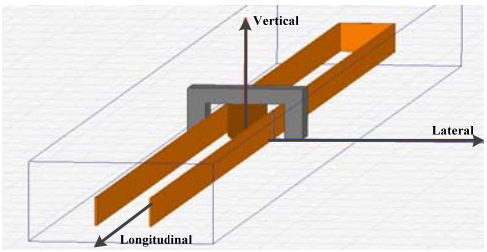

Fig. 5. The 3-D model of the movable ICPT system.

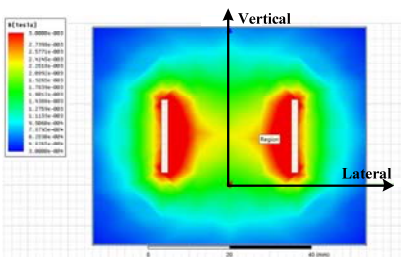

(a) Magnetic field distribution without secondary side.

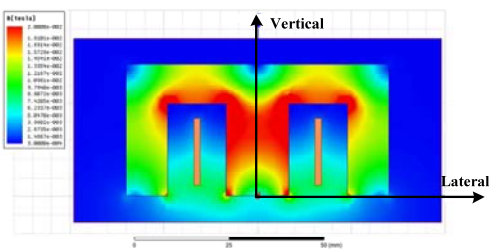

(b) Magnetic field distribution with secondary side.

Fig. 6. The magnetic field distribution of the movable ICPT system.

$$Z_{s2} = \omega_{os2} L_{s2} \frac{1 - \omega_{ns2}\lambda_{s2} + j\omega_{ns2} Q_{s2}[\lambda_{s2}(1-\omega^2{}_{ns2}) + 1]}{Q_{s2}(1-\omega^2{}_{ns2}) + j\omega_{ns2}} \tag{12}$$

The primary equivalent circuit model is redrawn with the secondary reflecting impedance in Fig. 7(b), where Z_{ps1} and Z_{ps2} are defined as:

$$Z_{ps1} = \frac{(\omega M_1)^2}{Z_{s1}} \tag{13}$$

$$Z_{ps2} = \frac{(\omega M_2)^2}{Z_{s2}} \tag{14}$$

Likewise, the secondary circuit model can be easily deduced as presented in Fig. 7(c). The voltage u_{sk} (k=1, 2) is induced by

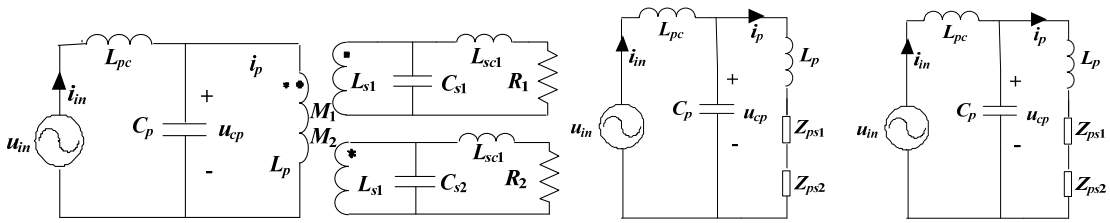

(a) Mutual inductance model. (b) Primary equivalent model. (c) Secondary equivalent model (k=1,2).

Fig. 7. The equivalent circuit of movable ICPT with two loads.

the primary current i_p, whose RMS value can be expressed as

$$U_{sk} = \omega M_k I_p \quad (k=1,\ 2) \tag{15}$$

where I_p stands for the RMS value of the primary current i_p.

C. Demands of the Compensation Circuit

The movable ICPT system with a multi-load has the following two characteristics: 1) increasing the amplitude and frequency of the primary current to improve the transfer power due to a low coupling coefficient between the primary side and the secondary sides; 2) guaranteeing each secondary side under stand-alone operation.

1) The Primary Side and Secondary Sides are Controlled Independently: As can be seen from expression (15), if the mutual inductance is constant, keeping ω and I_p constant will ensure the induced the voltage U_{sk} to be constant in the secondary coils. Then, each secondary side can operate independently. This method, controlling the primary side and the secondary sides separately, can make every secondary side work independently and remove the feedback loop between the secondary sides and the primary side.

2) The Secondary Reflected Impedances in Primary Side are Pure Resistive: If the reflected impedance in the primary side is inductive or capacitive, the primary resonant frequency will be forced to change and the reactive power will increase. Therefore, the secondary input impedance should be kept pure resistive when designing the secondary compensation.

3) The Primary Compensation Measure Aims at Reducing the Reactive Power: As shown in Fig. 7(b), the large current in the primary side is generated by the resonance of C_p and L_{pc}. In order to decrease the current flowing from C_p to the source, the value of L_{pc} has to be improved. Although a larger L_{pc} decreases the transfer power, it can reduce the reactive power effectively and achieve soft-switching more easily.

IV. Design of the LCL Resonant Compensation

A. Secondary LCL Compensation Design

From equation (8), only when λ=1 and ω_n=1 is it possible for the LCL circuit to achieve a constant current output and a pure resistive input impedance.

$$\begin{cases} \omega_{osk} = \omega \\ L_{sck} = L_{sk} \\ C_{sk} = 1/\left(\omega_{osk}{}^2 L_{sck}\right) \end{cases} \quad (k=1, 2) \tag{16}$$

For this, the above conditions must be met during the design of the secondary LCL compensation. Then, the output current can be written as:

$$I_{ok} = \frac{M_k}{L_{sk}} I_p \tag{17}$$

The output power can be expressed by:

$$P_{oLCLk} = I_{ok}^2 R_k = (\frac{M_k}{L_{sk}} I_p)^2 R_k \tag{18}$$

The relationship between the secondary output power and the primary current RMS current is shown in Fig. 8. When I_p=50A and R_1=R_2=40Ω, the total output power of the secondary sides is about 50W. Hence, the primary RMS current is selected as 50A.

B. Comparison of the Secondary LCL Compensation and the Series Compensation

If LCR series circuit resonates, the input impedance is pure resistive and the output voltage is equal to the input voltage. The equivalent circuit of the series resonance compensation circuit in the secondary side is shown in Fig. 9.

While resonating, the RMS value of the output voltage is:

$$U_{os} = U_{sk} = \omega M_k I_p \tag{19}$$

The output power can be derived and written as:

$$P_{os} = \frac{U_{os}{}^2}{R_k} = \frac{\left(\omega M_k I_p\right)^2}{R_k} \tag{20}$$

Comparing (18) to (20), the power ratio can be achieved by:

$$\gamma = \frac{P_{os}}{P_{oLCLk}} = \left(\frac{\omega L_{sk}}{R_k}\right)^2 = Q_{sk}{}^2 \tag{21}$$

As shown in (21), when the Q-value of the secondary side Q_{sk}>1, the output power of the series compensation is larger than that of the LCL compensation. However, the LCL compensation can achieve much more power when Q_{sk}<1. This is obvious in Fig. 10.

C. Primary LCL Compensation Design

Taking the LCL compensating secondary side as an

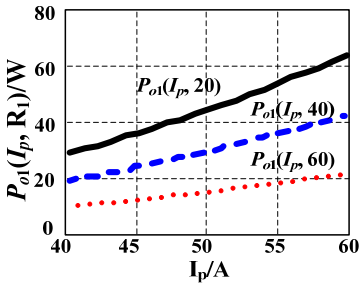

(a) The output power of the first secondary side.

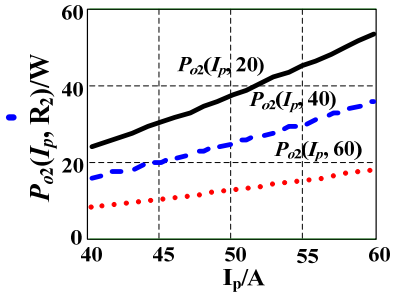

(b) The output power of the second secondary side.

Fig. 8. The relation between the secondary output power and the primary RMS current.

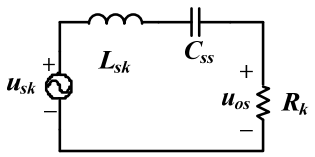

Fig. 9. The equivalent circuit of series resonance compensation circuit in the secondary side.

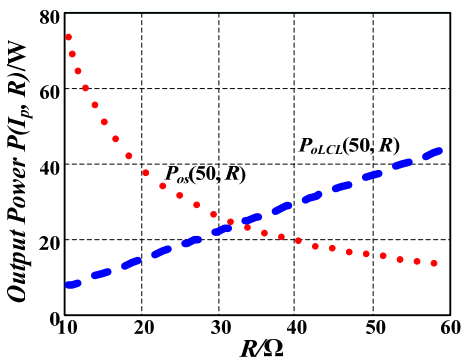

Fig. 10. The relationship of the output power and the load resistance when I_p=50A.

example, the secondary equivalent load in the primary side can be derived through (13) and (14):

$$R_{eq} = Z_{ps1} + Z_{ps2} = \left(\frac{M_1}{L_{s1}}\right)^2 R_1 + \left(\frac{M_2}{L_{s2}}\right)^2 R_2 \qquad (22)$$

Consequently, the primary equivalent circuit in Fig. 7(b) can be converted to a new model as shown in Fig. 11(a).

From the analysis in Chapter 3 Section C Point 3, the primary ratio of the inductors λ_p needs to be large enough (λ_p>10). In this case, the primary equivalent circuit is

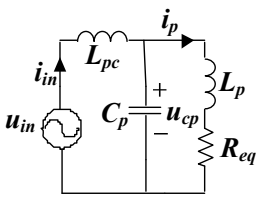

(a) Primary equivalent circuit.

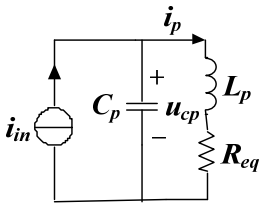

(b) Primary LCR parallel equivalent circuit.

Fig. 11. The equivalent circuit of the primary side.

transformed into the LCR parallel circuit according to Chapter 2 Point 2, as shown in Fig. 11(b). Due to the very low coupling coefficient of this movable ICPT system, the values of M_k/L_{sk} and R_{eq} are very small. From expression (9), the primary approximate resonant angular frequency can be further simplified to:

$$\omega_{op} \approx 1/\sqrt{L_p C_p} \qquad (23)$$

Combining the limitation of (10), the range of the primary load (i.e. secondary equivalent load) can be given by:

$$R_{eq} < \sqrt{L_p/C_p} \qquad (24)$$

which determines the maximum load that the secondary sides are able to carry. The secondary equivalent loads in the primary side must satisfy equation (24) during the design process.

The primary input apparent power is discussed by the following expression:

$$S = \left\{\frac{Q_p\left(1-\omega_{np}^{\ 2}\right)+j\omega_{np}}{1-\omega_{np}^{\ 2}\lambda_p + j\omega_{np}Q_p\left[\lambda_p\left(1-\omega_{np}^{\ 2}\right)+1\right]}\right\} \frac{1+j\omega_{np}Q_p}{1-\omega_{np}^{\ 2}\lambda_p + j\omega_{np}Q_p\left[\lambda_p(1-\omega_{np}^{\ 2})+1\right]} \frac{U_{in}^{\ 2}}{\omega_{op}L_p} \qquad (25)$$

Obviously, the input active power is P=Re(S), and the input reactive power is Q=Im(S). By a Mathcad calculation, the relationships among the input power, the primary normalized angular frequency ω_{np}, and the ratio of the inductors λ_p is shown in Fig. 12. P and Q present the input active power and the input reactive power, respectively; D is the duty cycle of the input voltage source; and R_1 and R_2 are the load resistors in the secondary sides.

As can be seen from Fig. 12, as λ_p increases, the maximum value of the input active power decreases. However, the maximum input active power point is close to the position where ω_{np}=1. This means that the operating frequency closest to the angular resonant frequency and the input impendence is nearly pure resistive, which will increase the input power factor. For this reason, the operating frequency is set at the point of ω_{np}=1, and λ_p =60 is chosen for the purpose of achieving a 50W transfer power.

Considering that the primary normalization frequency ω_{np} is set at ω_{np}=1, the relationships among the primary RMS current

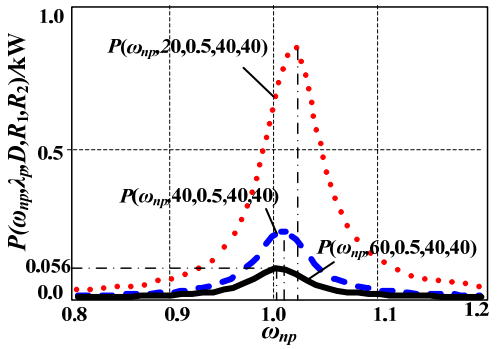

(a) Active power.

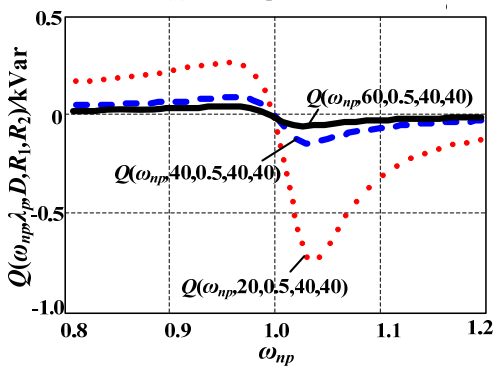

(b) Reactive power.

Fig. 12 The relationships among the input power, the primary normalized angular frequency ω_{np}, the ratio of inductors λ_p.

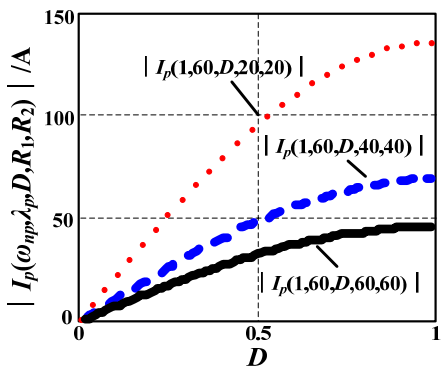

(a) The curves of I_p and D.

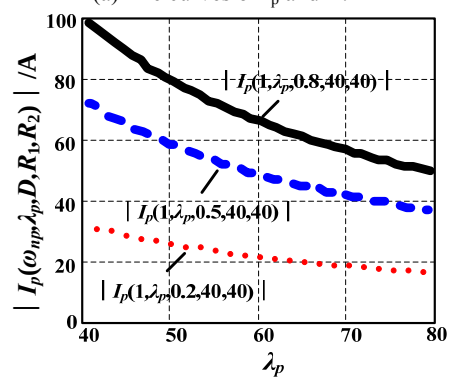

(b) The curves of I_p and λ_p.

Fig. 13. The relationships among the primary RMS current I_p, the duty cycle D, and the ratio of inductors λ_p.

I_p, the load resistance, the duty cycle D, and the ratio of the inductors λ_p is researched here. In Fig. 13 (a), the inductor ratio λ_p is kept constant while the two load resistances are 20Ω, 40Ω, and 60Ω and the duty cycle D varies from 0 to 1. In Fig. 13 (b), the load resistance is kept constant while the duty cycle D is 0.2, 0.5, and 0.8 and the ratio of the inductors λ_p changes from 40 to 80. From the curves in Fig.13, the primary RMS current is 50A when R_1=R_2=40Ω, D=0.5, and λ_p=60, which corresponds with the previous analysis.

D. Design Method

According to former research, the design method of the LCL compensation in a constant-current movable ICPT system with a multi-load is summarized as follows:

1) The resonant angular frequency of each secondary side and the primary side are equal to the operating frequency.

$$\omega = \omega_o = \omega_{op} = \omega_{osk} \tag{26}$$

2) The secondary ratio of the inductors λ_{sk} in the LCL compensation should be set at 1.

$$L_{sck} = L_{sk} \tag{27}$$

3) The primary RMS current I_p is determined by the secondary output power as shown in Fig. 7.

4) The primary ratio of the inductors λ_p in the LCL compensation is conditioned by the primary RMS current I_p and the duty cycle D at the steady state, which can determine the value of the primary compensation inductor as shown in Fig. 10.

5) According to the resonant angular frequency and the values of the inductors, the values of the primary and secondary compensation capacitors can be calculated by following equations:

$$C_{sk} = 1/\omega_o^2 L_{sk} \quad (k=1,\ 2) \tag{28}$$

$$C_p = 1/\omega_o^2 L_p \tag{29}$$

V. Experimental Results

A. Experiment Platform

According to the schematic diagram in Fig. 14, the platform is constructed with f=25kHz, λ_p=60, where the inverter topology is a phase-shifted full-bridge circuit.

On this platform, the PWM control strategy has been adopted to realize the constant-current characteristic as shown in Fig. 15. The primary side control and the secondary side control are independent of each other. In the primary side, the current control is used to make the primary RMS current constant; and in the secondary sides, the control strategy and the converter topology are chosen according to the load units which are replaced by resistors here. Generally, a load unit contains a power electronic converter, electric equipment and a control unit.

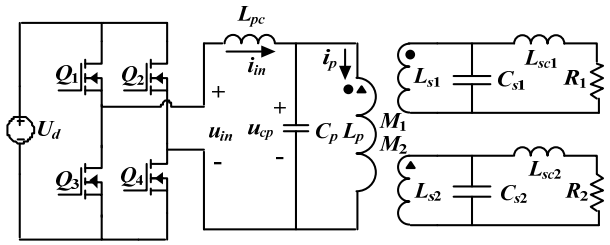

Fig. 14. The simulation and experiment circuit diagram.

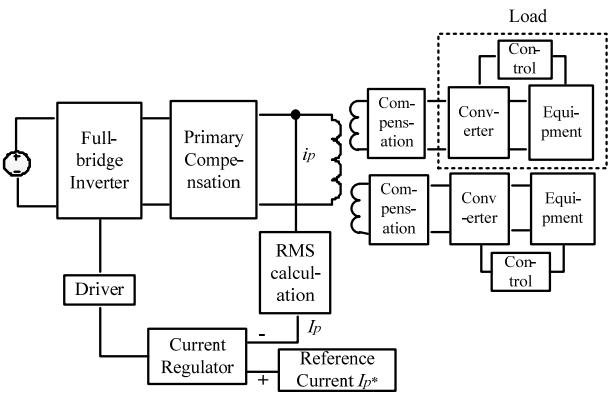

Fig. 15. The control block diagram of the movable ICPT system with multi-load.

TABLE I
SIMULATION AND EXPERIMENT PARAMETERS

Parameter	Value	Parameter	Value
U_d	100V	L_{pc}	60uH
L_p	1.0uH	L_{sc1}	205.4uH
L_{s1}	206.4uH	L_{sc2}	233.5uH
L_{s2}	230.7uH	C_p	40uF
M_1	3.56uH	C_{s1}	0.19uF
M_2	3.65uH	C_{s2}	0.17uF

The parameters of the simulation and experiment are listed in Table I.

As shown in Fig. 16 (a), the primary rail is constructed with a copper sheet (18mm*0.4mm) by four layers parallel winding, which is packed and fixed by an insulating plate. The interval of the guide rail is set in accordance with the size of the secondary pick-ups. In Fig. 16 (b), the secondary pick-ups employ E-Type cores with 43 and 45 turns (d=1mm) wound on their central columns. The pick-ups can ride on the primary rail and slide freely.

B. Experiment Results

To verify the effectiveness of the analyses of the LCL compensation, experiments were performed using the designed ICPT system, which contains a one-meter rail (as the primary side). Fig. 17-Fig. 21 exhibit the experiment results.

Fig. 17 shows the tendency of the output current affected by the load when the secondary side is compensated by the LCL circuit. Although R_1 changes, the output current is approximately constant, i.e., the constant current output characteristic is obtained.

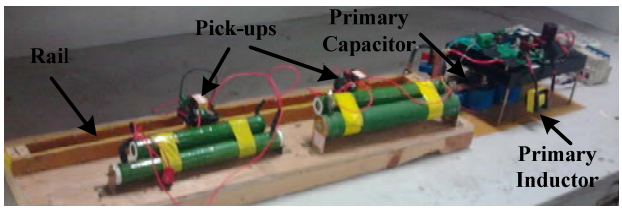

(a) The experiment platform.

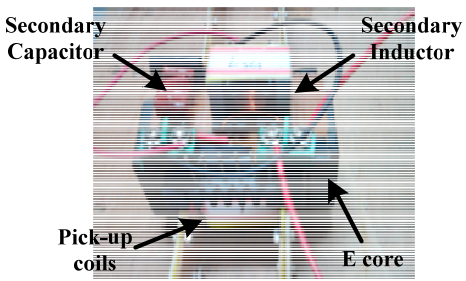

(b) The pick-up structure.

Fig. 16. The movable ICPT system with multi-load platform.

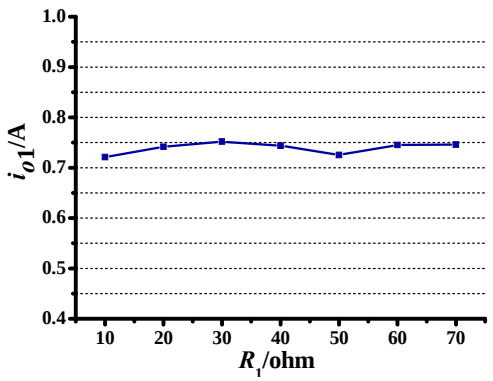

Fig. 17. The output current with LCL compensation circuit in the secondary side.

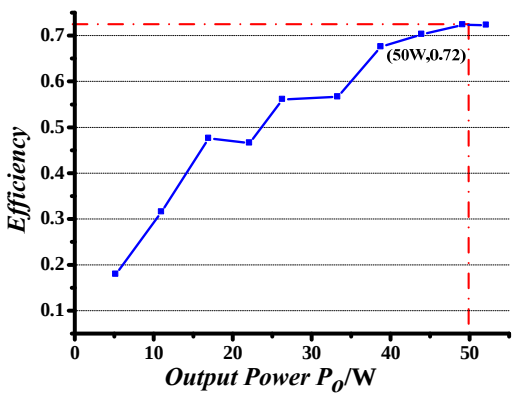

Fig. 18. The efficiency of the system.

The efficiency of the LCL compensating ICPT system varying with the output power is shown in Fig. 18. Obviously, the efficiency improves with an increase of the output power, and reaches its maximum value of 72% at the 50W-point.

The characteristic of the secondary series compensation is different from the secondary LCL compensation as shown in

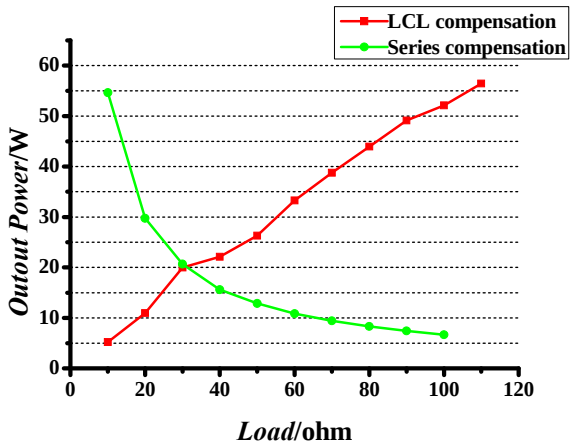

Fig. 19. The output power of LCL and series compensation circuits in the secondary side.

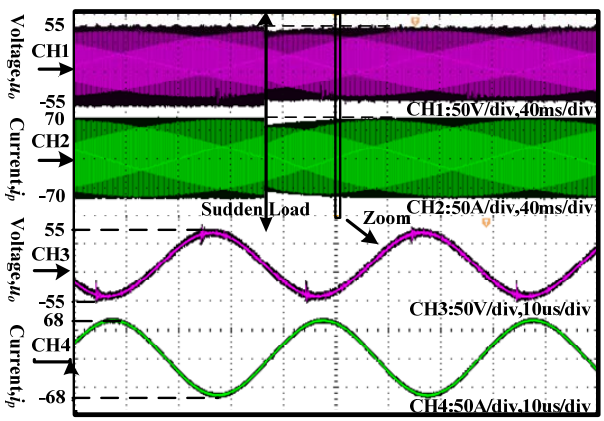

Fig. 20. The waveforms of u_{o1} and i_p with sudden load.

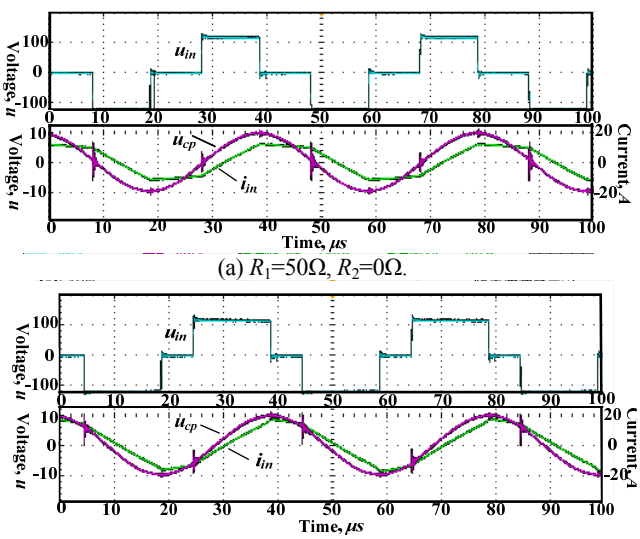

(a) R_1=50Ω, R_2=0Ω.

(b) R_1=50Ω, R_2=50Ω.

Fig. 21. The waveforms of the input voltage u_{in}, the input current i_{in}, and the primary capacitor voltage u_{cp} with changing load.

Fig. 19. Obviously, in the case of an increasing load, the secondary LCL compensation is superior to the secondary series compensation.

When R_2 is suddenly added to the system, the voltage u_{o1} of the load R_1 and the primary current i_p will change as shown in Fig. 20. In the instant of the load rising up, the amplitudes of u_{o1} and i_p decline first. Then with the closed-loop PWM control, the duty cycle of the input voltage will increase and eventually both u_{o1} and i_p return to their initial values.

Fig. 21 shows the waveforms of the input voltage u_{in}, the input current i_{in}, and the primary compensation capacitor voltage u_{cp} when the load changes. From Fig. 21, it can be seen that when

the load resistance increases, the duty cycle of u_{in} increases and the phase deviation between u_{cp} and i_{in} decreases, which lead to an increase of the input active power.

VI. Conclusions

This paper draws a conclusion that keeping the frequency and amplitude of the primary current constant can make each load operate independently when the mutual inductance does not change.

For a complex ICPT system with a large-inductor-ratio LCL compensation, this paper proposes a method to obtain an approximate resonant angular frequency. The system used in this paper is compensated by an LCL circuit in both the primary and secondary sides. The primary LCL compensation can lower the reactive power and generate a large current in the primary side. In addition, it can also suppress the harmonic current and realize soft switching. The secondary LCL circuit can increase the output power and achieve a constant current output. Simulation and experiments have been conducted to verify the effectiveness and accuracy of the theory and design method.

It needs to be pointed out that due to an almost constant mutual inductance in this movable ICPT system, there is no consideration for variable mutual inductance situations, which is a deficiency of this paper.

References

[1] C.-G. Kim, D.-H. Seo, J.-S. You, and J.-H. Park, "Design of a contactless battery charger for cellular phone," *IEEE Trans. Ind. Electron.*, Vol. 48, No. 6, pp. 1238-1247, Dec. 2001.

[2] C.-S. Wang, O. H. Stielau, and G. A. Covic, "Design considerations for a contactless electric vehicle battery charger," *IEEE Trans. Ind. Electron.*, Vol. 52, No. 5, pp. 1308-1314, Oct. 2005.

[3] W. Zhou and H. Ma, "Design considerations of compensation topologies in ICPT system," *Applied Power Electronics Conference. APEC 2007 - Twenty Second Annual IEEE*, pp. 985-990, Feb./Mar. 2007.

[4] F. Huang and J. Wang, "Investigation on full bridge inductively coupled power transfer system," *Power Electronics and Motion Control Conference (IPEMC). 2012 7th International*, Vol. 3, pp. 1737-1740, Jun. 2012.

[5] Y. X. Xu, J. T. Boys, and G. A. Covic, "Modeling and

controller design of ICPT pick-ups," *Power System Technology. 2002. Proceedings. PowerCon 2002. International Conference*, Vol. 3, pp.1602-1606, 2002.
[6] J. T. Boys, G. A. Covic, and Y. Xu, "DC analysis technique for inductive power transfer pick-ups," *IEEE Power Electron Lett.*, Vol. 1, No. 2, pp. 51-53, Jun. 2003.
[7] J. T. Boys, G. A. Covic, and A. W. Green, "Stability and control of inductively coupled power transfer systems," *Proceeding of IEE Electric Power Applications*, Vol. 147, No. 1, pp. 37-43, Jan. 2000.
[8] M. Borage, S. Tiwari, S. Kotaiah, "Analysis and design of an LCL-T resonant converter as a constant-current power supply," *IEEE Trans. Ind. Electron.*, Vol. 52, No. 6, pp. 1547-1554, Dec. 2005.
[9] A. K. S. Bhat, "Analysis and design of LCL-type series resonant converter," *IEEE Trans. Ind. Electron.,* Vol. 41, No. 1, pp. 118-124, Feb. 1994.
[10] C.-S. Wang, G. A. Covic, and O. H. Stielau, "Investigating an LCL load resonant inverter for inductive power transfer applications," *IEEE Trans. Power Electron.*, Vol. 19, No. 4, pp. 995-1002, Jul. 2004.
[11] N. Keeling, G. A. Covic, F. Hao, and L. George, "Variable tuning in LCL compensated contactless power transfer pickups," *Energy Conversation Congress and Exposition. San Jose, CA: IEEE*, pp. 1826-1832, Sep. 2009.
[12] C.-Y. Huang, J. T. Boys, and G. A. Covic, "LCL pick-up circulating current controller for inductive power transfer systems," *IEEE Trans. Power Electron.,* Vol. 28, No. 4, pp. 2081-2093, Apr. 2013.
[13] G. A. Covic, J. T. Boys, A. M. W. Tam, and J. C.-H. Peng, "Self tuning pick-ups for inductive power transfer," *Power Electronics specialists Conference*, pp. 3489-3494, Jun. 2008.
[14] X. Dai, Y. Zou, and Y. Sun, "Uncertainty modeling and robust control for LCL resonant inductive power transfer system," *Journal of Power Electronics*, Vol. 13, No. 5, pp. 814-828, Sep. 2013.

Jie Hua was born in China, in 1991. She received her B.S. degree from the Department of Automation Engineering, Nanjing University of Aeronautics and Astronautics, Nanjing, China, in 2013. She is presently working toward her M.S. degree in Automation Engineering from the Nanjing University of Aeronautics and Astronautics. Her current research interests include inductive contactless power transfer systems.

Hui-Zhen Wang was born in China, in 1964. She received her B.S. degree from the Department of Electrical Engineering, Nanjing Aeronautical Institute, Nanjing, China, in 1983. She is presently a Professor in the College of Automation Engineering, Nanjing University of Aeronautics and Astronautics, Nanjing, China. She is the holder of 13 Chinese invention patents. Her current research interests include power electronics and the control of electrical machines. Professor Wang was a recipient of a Second Prize of the State Technology Invention Award.

Yao Zhao was born in China, in 1987. He received his B.S. degree in Automation from Anhui University, Hefei, China, in 2009, and his M.S. degree in Electrical Engineering from the Shanghai Maritime University, Shanghai, China, in 2011. He is presently working toward his Ph.D. degree in Automation Engineering at the Nanjing University of Aeronautics and Astronautics, Nanjing, China. His current research interests include doubly salient electrical machines for aircraft power and electric vehicles, and new energy generation systems.

Ai-Long Zou was born in China, in 1988. He received his B.S. degree in Automation Engineering from Hohai University, Nanjing, China, in 2011, and his M.S. degree in Automation Engineering from the Nanjing University of Aeronautics and Astronautics (NUAA), Nanjing, China, in 2014. From 2011 to 2014, he studied wireless power transfer (WPT). Since 2014, he has been working on WPT and active power filters in the 724 research institute of the China Shipbuilding Industry Corporation, Beijing, China.